

1 **Predicting aboveground biomass in Arctic landscapes using very high**
2 **spatial resolution satellite imagery and field sampling**

3 Aleksi Räsänen, corresponding author

4 *Ecosystems and Environment Research Programme, Faculty of Biological and*
5 *Environmental Sciences, and Helsinki Institute of Sustainability Science (HELSUS),*
6 *P.O Box 65, FI-00014 University of Helsinki, Finland, aleksi.rasanen@helsinki.fi*

7 *Department of Geography, Norwegian University of Science and Technology, NO-7491*
8 *Trondheim, Norway*

9 Sari Juutinen

10 *Ecosystems and Environment Research Programme, Faculty of Biological and*
11 *Environmental Sciences, and Helsinki Institute of Sustainability Science (HELSUS),*
12 *P.O Box 65, FI-00014 University of Helsinki, Finland, sari.juutinen@helsinki.fi*

13 Mika Aurela

14 *Finnish Meteorological Institute, PO Box 503, FI-00101 Helsinki, Finland,*
15 *mika.aurela@fmi.fi*

16 Tarmo Virtanen

17 *Ecosystems and Environment Research Programme, Faculty of Biological and*
18 *Environmental Sciences, and Helsinki Institute of Sustainability Science (HELSUS),*
19 *P.O Box 65, FI-00014 University of Helsinki, Finland, tarmo.virtanen@helsinki.fi*

20 word count: 9383

21

22 **Predicting aboveground biomass in Arctic landscapes using very high** 23 **spatial resolution satellite imagery and field sampling**

24 Remote sensing based biomass estimates in Arctic areas are usually produced
25 using coarse spatial resolution satellite imagery, which is incapable of capturing
26 the fragmented nature of tundra vegetation communities. We mapped
27 aboveground biomass using field sampling and very high spatial resolution
28 (VHSR) satellite images (QuickBird, WorldView-2 and WorldView-3) in four
29 different Arctic tundra or peatland sites with low vegetation located in Russia,
30 Canada, and Finland. We compared site-specific and cross-site empirical
31 regressions. First, we classified species into plant functional types and estimated
32 biomass using easy, non-destructive field measurements (cover, height). Second,
33 we used the cover/height-based biomass as the response variable and used
34 combinations of single bands and vegetation indices in predicting total biomass.
35 We found that plant functional type biomass could be predicted reasonably well
36 in most cases using cover and height as the explanatory variables (adjusted R^2
37 0.21–0.92), and there was considerable variation in the model fit when the total
38 biomass was predicted with satellite spectra (adjusted R^2 0.33–0.75). There were
39 dissimilarities between cross-site and site-specific regression estimates in satellite
40 spectra based regressions suggesting that the same regression should be used only
41 in areas with similar kinds of vegetation. We discuss the considerable variation in
42 biomass and plant functional type composition within and between different
43 Arctic landscapes and how well this variation can be reproduced using VHSR
44 satellite images. Overall, the usage of VHSR images creates new possibilities but
45 to utilize them to full potential requires similarly more detailed in-situ data
46 related to biomass inventories and other ecosystem change studies and modelling.

47 **1. Introduction**

48 Biomass is a key parameter for tracking plant productivity, which is central to the flow
49 of energy and nutrients in an ecosystem (Epstein et al. 2012; van der Wal and Stien
50 2014). In Arctic tundra and other northern landscapes with low-growth vegetation,
51 knowledge of the biomass distribution is a prerequisite for understanding and mapping
52 changes in key ecosystem parameters such as the carbon cycle and permafrost dynamics

53 (Chen, Li, et al. 2009; Epstein et al. 2012). Biomass patterns have been estimated for
54 decades using satellite images which allow the mapping of vast areas with little field
55 work (Laidler and Treitz 2003; Raynolds, Walker, and Maier 2006; Epstein et al. 2012;
56 Buchhorn, Raynolds, and Walker 2016).

57 In Arctic environments, satellite based estimates of biomass distribution have
58 mostly been carried out using rather coarse spatial resolution images (Walker et al.
59 2003; Heiskanen 2006; Raynolds, Walker, and Maier 2006; Epstein et al. 2012;
60 Raynolds et al. 2012; Buchhorn et al. 2013; Doiron et al. 2013; Johansen and
61 Tommervik 2014; Berner et al. 2018), such as Landsat (30 m pixel size) (Heiskanen
62 2006; Johansen and Tommervik 2014; Berner et al. 2018), MODIS (250 m pixel size)
63 (Westergaard-Nielsen et al. 2015), and AVHRR (>1 km pixel size) (Walker et al. 2003;
64 Raynolds, Walker, and Maier 2006; Epstein et al. 2012; Raynolds et al. 2012; Buchhorn
65 et al. 2013; Doiron et al. 2013). Although the images with coarse spatial resolution have
66 high temporal resolution and they have proved to be suitable for circumpolar studies
67 and detecting coarse-scale biomass patterns (coefficient of determination (R^2) up to
68 0.89) (Walker et al. 2003), they are incapable of representing the fragmented nature of
69 tundra environment and fine-scale changes in vegetation and carbon dynamics (Laidler
70 and Treitz 2003; Virtanen and Ek 2014; Siewert et al. 2015; Beamish et al. 2017).

71 Very high spatial resolution (VHSR, spatial resolution 0.5–2.5 m) satellite
72 images could offer a potential method to map landscape-scale biomass distribution in an
73 ecologically sound pixel size (Laidler and Treitz 2003; Virtanen and Ek 2014). In
74 addition, field data is usually collected in small plots, which are more comparable to the
75 pixel size of VHSR than coarser resolution imagery. However, the use of VHSR images
76 has been modest in biomass prediction (Fuchs et al. 2009; Atkinson and Treitz 2013;
77 Collingwood et al. 2014; Greaves et al. 2016). In Canadian tundra landscapes,

78 reasonably high prediction capabilities (R^2 of 0.55 to 0.79) have been obtained with
79 VHSR images (Atkinson and Treitz 2013; Collingwood et al. 2014). When reflectance
80 data are combined with other types of data, such as radar and topographical data (Chen,
81 Blain, et al. 2009; Collingwood et al. 2014) or LiDAR (Greaves et al. 2016), higher
82 explanatory power can be obtained. The use of VHSR satellite imagery, radar and
83 LiDAR data is hampered by the low availability of such data in VHSR at the global
84 scale (Sinha et al. 2015; Steele-Dunne et al. 2017), and logistical and practical issues
85 limit data collection possibilities with remotely piloted aircraft systems in remote Arctic
86 locations. Nevertheless, the use and availability of LiDAR, radar, and VHSR optical
87 images is increasing and they present an interesting research frontier in Arctic
88 vegetation studies. So far, to the best of our knowledge, there are no studies in which
89 biomass has been estimated using VHSR data and compared in various tundra
90 environments across the circumpolar Arctic, although there have been calls for biome-
91 wide observation methodologies (Walker et al. 2016). Therefore, there is a need to test
92 whether cross-site biomass models that include data from divergent Arctic landscapes
93 can be developed.

94 To get field validation data for remote sensing studies, harvested biomass
95 samples at a plot scale are needed (Hope, Kimball, and Stow 1993; Walker et al. 2003;
96 Reynolds, Walker, and Maier 2006; Kushida et al. 2015; Greaves et al. 2016).
97 Previously, it has been suggested that non-destructive methods, such as estimations of
98 height, %-cover and volume of plant species or plant functional types (PFTs, which are
99 groups of plants with functional similarity and similar growth form), are sufficient for
100 estimating plot-scale biomass in landscapes with low-growth vegetation and allow the
101 collection of larger validation sets (Chen, Li, et al. 2009; Axmanova et al. 2012;
102 Suvanto, Le Roux, and Luoto 2014). Also in this case, models have been developed and

103 applied only in one specific location and studies that test whether one model can be
104 applied in various tundra environments are lacking.

105 Our objective was to predict biomass distribution by using VHRS satellite
106 imagery in different Arctic tundra and peatland communities and evaluate whether the
107 same predictive regressions can be applied across circumpolar Arctic sites. Therefore, in
108 this study, we first estimated PFT-specific biomass using harvested biomass as the
109 response variable and field-measured height and %-cover as predictors. Second, we
110 estimated total biomass using modelled cover/height-based biomass as the response
111 variable and single bands and vegetation indices of VHRS satellite images as predictors.
112 At both steps, we compared different predictor combinations and transformations as
113 well as site-specific and cross-site regressions. We concluded our study by discussing
114 how general the regressions are for biomass prediction and how different PFTs
115 contribute to biomass across circumpolar northern landscapes with low-growth
116 vegetation.

117 **2. Materials and methods**

118 *2.1. Study sites*

119 We included four different study sites which present a continuum from northern boreal
120 to sub-Arctic and to Arctic landscapes: Sodankylä in Finland, northwestern (NW)
121 Russia, Herschel in Canada and Tiksi in Russia (Figures 1 and 2, Table 1). All the study
122 sites are characterized by low-growth vegetation, but having some variation in
123 landscape patterns and vegetation communities, which make them a good combination
124 for a circumpolar comparison and testing whether simple and general approach could be
125 used for spatial modelling.

126 [FIGURE 1 approximately here]

127 [FIGURE 2 approximately here]

128 [TABLE 1 approximately here]

129 The Sodankylä study site is an open north-boreal fen in northern Finland (Figure
130 1). The vegetation pattern consists of strings with shrubs and birch trees, and lawns and
131 flarks with *Sphagnum* and brown mosses and sedges (Figure 2a, see Appendix 1 in the
132 supplemental material for the dominant species). For further site description see
133 (Dinsmore et al. 2017).

134 The study sites Khosedayu, Rogovaya 1 and 2, and Seida located in NW Russia
135 within 150 km to each other near the Ural Mountains (Figure 1). Generally, the
136 vegetation, geomorphology, climate and soil characteristics were similar in these four
137 sites; therefore, they are analyzed together. The vegetation belongs to the ecotone of
138 forest-tundra – tundra zones, and is a mosaic of peatlands, heaths with different kind of
139 shrubs and willow thickets and meadows along streams (Figure 2b, Appendix 1 in the
140 supplemental material, see also Hugelius et al. (2011) and Virtanen and Ek (2014)).

141 The Canadian study site is located on Herschel Island, which has an area of
142 approximately 100 km² and is located a few kilometres off the Yukon Coast in the
143 southern Beaufort Sea, Canada (Figure 1). Prominent geomorphic features are smooth
144 hills, river channels, and numerous retrogressive thaw slumps. In the lowland tundra,
145 there are several different herb rich plant community types but also other type of
146 vegetation (Figure 2c, Appendix 1 in the supplemental material, see also (Myers-Smith
147 et al. 2011) and (Obu et al. 2017)).

148 The Tiksi study site is located near the coast of the Laptev Sea about 120 km
149 southeast of the Lena River delta in Siberia, Russia (Figure 1). The site consists of
150 relatively flat lowlands and gently sloping hillslopes with elevations at 200–300 m a.s.l.
151 Sedge and moss dominated peatlands, tundra heaths with low shrubs, and rocky and

152 lichen covered surfaces alternate in the site (Figure 2d, Appendix 1 in the supplemental
153 material, see also Grosswald et al. (1992), Juutinen et al. (2017) and Mikola et al.
154 (2018)).

155 ***2.2. Biomass field data***

156 We measured the biomass, %-cover and height of the following PFTs: (1) dwarf shrubs,
157 (2) herbs, (3) graminoids, (4) dwarf birch (*Betula nana*), (5) *Salix spp.* and other tall
158 shrubs (height ≤ 1.5 m), and (6) mosses (height not measured). Examples of the
159 common species or genera included in each PFT for each study site are listed in
160 Appendix 1 in the supplemental material. The PFT classification we used was a slight
161 modification of the one presented by Chapin III et al. (1996), and was used earlier at
162 one of the study sites (Hugelius et al. 2011).

163 In each study site, we sampled 48 to 182 circular plots either randomly or using
164 transects (Table 1, Appendix 3 in the supplemental material). When sampling, plots of
165 each major vegetation type were included, and plots were representative of the
166 overall landscape in each study site. Sampling set-up differed between study sites,
167 because data were collected during different field campaigns and projects over several
168 years. Field plots were classified in the field into vegetation types which were defined in
169 previous studies in each site (Smith et al. 1989; Virtanen and Ek 2014; Juutinen et al.
170 2017; Obu et al. 2017). Each plot had a radius of 5 meters and contained 3 or 4
171 rectangular subplots of sides 30–50 cm in length (depending on the study site). These
172 subplots were located 1.0–2.5 m from the plot centroid at right angles to each other. We
173 visually estimated the %-cover of each PFT and measured the mean height of each PFT
174 using a ruler in each subplot. One of the subplots was harvested during the peak
175 growing season to measure aboveground biomass. All vascular plant material was
176 collected. For mosses, we collected a subsample of 5 cm x 5 cm with variable depths,

177 determined by the height of photosynthesizing part of the mosses. The harvested
178 biomass was sorted by PFT, oven dried at 60°C for 24 hours, and weighed. In
179 Sodankylä and NW Russia, i.e. sites with scattered trees (height > 1.5 m), tree biomass
180 in 5 m radius circular plots was calculated on the basis of tree height, mean stem
181 diameter at breast height and basal area by using allometric equations (Nyysönen 1955;
182 Varmola and Vuokila 1986; Alexeyev et al. 1995; Kauppi, Tomppo, and Ferm 1995;
183 Shepashenko, Shvidenko, and Nilsson 1998; Starr, Hartman, and Kinnunen 1998;
184 Korpela 2001) as specified in Appendix 2 in the supplemental material.

185 *2.3.Satellite imagery and its preprocessing*

186 From each study site, we used one cloud free QuickBird (2.4 m pixel size in
187 multispectral bands), WorldView-2 (2 m pixel size in multispectral bands), or
188 WorldView-3 (1.6 m pixel size in multispectral bands) VHSR satellite image (Digital
189 Globe, Westminster, CO, USA) acquired at approximately peak biomass and at
190 approximately the same time as the field work in the respective study sites (Table 1).

191 Generally, the temporal availability of VHSR satellite images is quite low in the
192 Arctic (Stow et al. 2004; Westergaard-Nielsen et al. 2013). Some of the images were
193 taken some days earlier in the summer than the field work, but these were the best
194 matching images at the time of image acquisition. In Tiksi and Seida, images were
195 taken some years before the field work but phenologically in a relatively similar phase
196 as the field work. This should not affect image interpretation due to small or lacking
197 disturbance and slow vegetation growth in these study sites. This interpretation is based
198 on our field observations, a MODIS trend analysis (Appendix 4 in the supplemental
199 material) and global comparisons in which only small changes have been observed in
200 these sites (Epstein et al. 2012; Myers-Smith et al. 2015). Nevertheless, the timing of

201 satellite images may produce some uncertainties in our analysis, and there might be
202 small-scale dynamics which cannot be observed in the MODIS images.

203 Satellite images were first atmospherically corrected and transformed to ground
204 reflectance values using the dark object subtraction method (Chavez 1988; Song et al.
205 2001). After atmospheric correction, images were orthorectified to match the field work
206 data. The geometric error based on our visual interpretations was a maximum of a
207 couple of meters. Due to lack of high precision GPS data or precisely georeferenced
208 maps or images, it was not possible to calculate the exact accuracy of the images.
209 However, the accuracy should be adequate, because we used 5 m radius circular plots
210 (plot area 78.5 m²) when predicting biomass with satellite images. In each plot, there
211 were between 13.6 (Quickbird) and 30.7 (WorldView-3) pixels. Satellite data values
212 were averaged to obtain a mean value per circular plot.

213 ***2.4.Data analysis overview***

214 We first estimated PFT-specific biomass using PFT %-cover and height measured in the
215 field as explanatory variables in the regression (referred as biomass-cover/height
216 regressions). Second, we used the predicted total biomass for each 5 m radius plot as the
217 response variable when developing regressions to estimate total aboveground biomass
218 distribution based on VHSR satellite images (referred as biomass-satellite spectra
219 regressions). For all sites and both regression steps, we tested both site-specific
220 regressions with data from one study site only and cross-site regressions in which data
221 from all study sites were used. As tree biomass was calculated using existing allometric
222 equations, biomass-cover/height regressions were not built for them, but they were
223 included in the biomass-satellite spectra regressions. We carried out all biomass-
224 cover/height and biomass-satellite spectra estimations with ordinary least squares linear
225 regressions. We acknowledge that there are also more sophisticated modelling

226 frameworks for biomass (Collingwood et al. 2014; Greaves et al. 2016) but our goal
227 was to test simple regression equations that can be easily interpreted and applied at
228 different sites. We performed data analyses in R 3.2.2. (R Core Team 2015), using the
229 car (Fox and Weisberg 2011), caret (Kuhn et al. 2016) and MASS (Venables and Ripley
230 2003) packages.

231 ***2.5.Plant functional group specific regressions for biomass based on*** 232 ***vegetation height and %-cover***

233 We predicted area-normalized PFT biomass for the subplots using the field measured
234 %-cover and average height of the respective groups in the subplot as explaining
235 factors. The data from harvested subplots were used to build the regressions. For all
236 variables, we tested the transformations suited to our data distribution in order to
237 achieve better normality for data and to find the best fitting regressions (McDonald
238 2014). For biomass and height, we used the following transformations (1) no
239 transformation, (2) square root, (3) natural logarithm + 1. For %-cover, we tried (1) no
240 transformation and (2) arcsine transformation ($\text{asin}(\sqrt{\text{\%-cover}/100})$), as %-cover
241 distribution varies between 0 and 1 (McDonald 2014).

242 For each functional group, we tried all the possible parameter combinations with
243 different transformations. We tested regressions with either one or both explanatory
244 variables but did not include two explanatory variables in the same regression if their
245 Pearson correlation was >0.7 . We formed the empirical relationships separately for each
246 study site and also carried out cross-site regressions. We evaluated the regressions based
247 on their root mean square error (RMSE) and chose the regressions with the lowest
248 RMSE value. Once the best regression was determined for each PFT, it was applied to
249 all subplots. Some of the regression equations had a negative intercept and predicted
250 negative biomass values for a small minority of the subplots. In these cases, the biomass

251 was set to 0 for the respective PFT in the subplot. Finally, we added up the biomass
252 values of every PFT to calculate the total biomass per area of each subplot. For some
253 functional groups at some sites (*Salix* spp. at Sodankylä and *Betula nana* on Herschel),
254 species were present only in one or two harvested subplots. In other situations, we did
255 not harvest biomass but measured PFT %-cover (mosses on Herschel). In these cases,
256 we used the cross-site biomass-cover/height regression estimations for the respective
257 functional groups when we summed up site-specific total biomass.

258 ***2.6. Predicting total biomass using VHSR satellite images***

259 We built biomass-satellite spectra regressions to predict biomass using estimated
260 cover/height-based total biomass as the response variable and individual spectral bands
261 and spectral indices of VHSR satellite images as predictors (Table 2). We carried out
262 three different types of regressions: site-specific cover/height predictions combined with
263 satellite image data from one site, cross-site cover/height predictions combined with
264 satellite image data from one site, and cross-site cover/height predictions with satellite
265 image data from all study sites.

266 [TABLE 2 APPROXIMATELY HERE]

267 Estimated cover/height-based biomass was calculated as the mean of the
268 predicted subplot biomass values in the respective 5 m radius plot. To evaluate the
269 uncertainty in biomass-cover/height regressions, we also carried out alternative
270 biomass-satellite spectra regressions, in which we used harvested subplot-scale biomass
271 data as response variable. In these alternative calculations, used site-specific
272 cover/height-based moss biomass estimate for Tiksi and Seida 2016 data and cross-site
273 cover/height-based moss biomass estimate for Herschel as mosses were not
274 systematically harvested in these datasets. For Sodankylä and NW Russia, we included
275 tree biomass in all biomass-satellite spectra regressions.

276 Individual spectral bands consisted of blue, green, red, and near infrared (NIR)
277 for the Quickbird images. For the WorldView images, the following bands were also
278 included: coastal, yellow, red-edge, and NIR2. We calculated the mean value per band
279 or index for the 5 m radius circle corresponding to each plot location.

280 We transformed biomass values with a natural logarithm as this transformation
281 has been used usually in tundra biomass studies, and it has been found in several studies
282 that there is a logarithmic relationship between biomass and satellite spectra (Walker et
283 al. 2003; Raynolds et al. 2012; Atkinson and Treitz 2013; Berner et al. 2018). Satellite
284 image values were not transformed. In each regression, those predictors whose
285 correlations were < 0.7 were chosen in the same model. All combinations were tested,
286 and also regressions with only one vegetation index. Variables were selected on the
287 basis of Akaike's Information Criteria and 10-fold cross-validation. Finally, we
288 compared the regressions built using different explanatory variable sets by comparing
289 the RMSE values.

290 **3. Results**

291 ***3.1. Aboveground biomass of different tundra and peatland vegetation types***

292 The highest total biomass values were found at the NW Russian sites consisting of both
293 mineral tundra and peatland. The southernmost site Sodankylä, a treeless fen, had lower
294 total biomass values than NW Russia study sites. The most Arctic site, Tiksi had the
295 lowest total biomass. The proportion of different PFTs varied among the study sites. At
296 Sodankylä, a major proportion of the biomass consisted of mosses; at NW Russia,
297 *Betula nana* and other shrubs had high biomass values; herbaceous biomass was higher
298 on Herschel than at other study sites, whereas at Tiksi, graminoids contributed most to
299 total biomass (when mosses were excluded) (Table 3). Similar trends could also be seen

300 in the average %-cover and height of PFTs, but there were variation in habitat type
301 specific biomass at each study site (Appendix 5 in the supplemental material). At
302 Sodankylä, there were trees in 32% (n = 16) of the 5 m radius plots with an average
303 biomass of 117.2 g m⁻², while at NW Russia trees were present in 6.8% (n = 25) of the
304 plots with an average biomass of 903.0 g m⁻².

305 [TABLE 3 APPROXIMATELY HERE]

306 ***3.2. Predicting biomass using easily measurable plant height and %-cover***

307 PFT-specific empirical regressions to predict biomass by %-cover and height of plants
308 performed well in most of the cases, with the adjusted coefficient of determination
309 (R^2_{adj}) values varying between 0.21 and 0.92 (Table 4). Overall, the lowest R^2_{adj} values
310 were obtained for mosses (R^2_{adj} 0.21–0.38), but also in some vascular plant regressions
311 RMSE values were relatively high. There was variation across study sites which PFT
312 regressions had the lowest RMSE and highest R^2_{adj} values.

313 [TABLE 4 APPROXIMATELY HERE]

314 Overall, the total predicted cover/height-based biomass values ranged between 0
315 and 2000 g m⁻² in the study plots (Figure 3). On average, the biomass was greatest and
316 had the largest variation at NW Russia. Based on site-specific estimate and excluding
317 trees, average total biomass was 423 g m⁻² and standard deviation 321 g m⁻². Sodankylä
318 had relatively high average biomass (282 g m⁻²) and low standard deviation (115 g m⁻²),
319 while Herschel (average 196 g m⁻², standard deviation 102 g m⁻²) and Tiksi (163 g m⁻²,
320 standard deviation 73 g m⁻²) had low average biomass values and low variation.

321 [FIGURE 3 APPROXIMATELY HERE]

322 Cross-site regressions performed quite differently between the study sites
323 (Figures 3 and 4), by underestimating total biomass on Herschel (21% difference) and at
324 NW Russia (2%), and overestimating at Sodankylä (10%) and at Tiksi (3%). At NW

325 Russia, PFT-specific average patterns between observed and predicted values were
326 close to 1:1 line, whereas at other study sites, there were more evident underestimation
327 or overestimation (Figure 4). NW Russia had the highest number of observations, which
328 may have an undue influence on the regression. In individual subplots and in PFTs,
329 disparities between cross-site and site-specific estimations were often significantly
330 higher than differences between average total site biomass.

331 [FIGURE 4 APPROXIMATELY HERE]

332 ***3.3. Using VHRSR imagery to estimate total aboveground biomass distribution***

333 In biomass-satellite spectra regressions, R^2_{adj} values ranged between 0.33 and 0.75
334 (Table 5). The best fits were obtained on Herschel and at Tiksi, whereas at Sodankylä
335 the R^2_{adj} values were seemingly low and at NW Russia RMSE values high. RMSE
336 values in cross-site biomass-satellite spectra regression were larger than in site-specific
337 biomass-satellite spectra regressions, with the RMSE value being especially high on
338 Herschel (Table 6). Cross-site biomass-satellite spectra regression overestimated
339 biomass values for Herschel, and underestimated for NW Russia and Tiksi (Figure 5,
340 Table 6). At Sodankylä, there was overestimation in plot-specific predicted values and
341 underestimation in the landscape (Table 6). Alternative biomass estimations having
342 harvested data as the response variable had higher RMSE values than biomass
343 estimations using cover/height-modelled biomass as the response variable. The
344 differences in average biomass values between regressions using cover/height-based
345 biomass estimate and harvested biomass were small at Sodankylä and Tiksi and a little
346 higher at NW Russia and on Herschel (Table 6). Finally, there was fine-scale spatial
347 variation in biomass distribution across the landscapes, and spatial pattern of biomass
348 was divergent in different study sites (Figure 6).

349 [TABLE 5 APPROXIMATELY HERE]

350 [TABLE 6 APPROXIMATELY HERE]

351 [FIGURE 5 APPROXIMATELY HERE]

352 [FIGURE 6 APPROXIMATELY HERE]

353 4. Discussion

354 Aboveground plant biomass in tundra environments can be predicted reasonably well at
355 the plot scale with easily measurable field data (height, %-cover) (Table 4, Figure 4).

356 This is also supported by the fact that biomass-satellite spectra regressions using
357 cover/height modelled biomass as the response variable had lower RMSE and relatively
358 similar average biomass estimate than biomass-satellite spectra regressions using
359 harvested biomass as the response variable (Table 6). The finding suggests that it is
360 more recommendable to measure plant cover and height in a larger area and estimate
361 biomass based on these measurements than to use only small harvested biomass
362 samples when carrying out biomass-satellite spectra models.

363 Previously, it has been shown that both %-cover and height information are
364 needed for the most accurate biomass predictions at the plot scale (Chen, Li, et al. 2009;
365 Axmanova et al. 2012; Suvanto, Le Roux, and Luoto 2014). Our results show instead
366 that in some sites and in some PFTs, the lowest RMSE values were obtained with %-
367 cover measurements only, but in most regressions for vascular plants, height
368 measurements were needed for the best predictions (Table 4). Biomass-cover/height
369 regressions had higher R^2_{adj} values for vascular plants than for mosses. The poor
370 regression performance of mosses compared to vascular plants could be related to small
371 size of harvested moss samples, to moisture content of the mosses as changing moisture
372 changes the volume, colour and productivity of mosses and to the heterogeneity of the
373 growth forms of moss genera. Possibly separate regressions for different types of
374 mosses, like liverworts, peat-mosses, and other mosses (possibly further divided into

375 sub-groups), should be used. In future studies, more samples in a more systematic way
376 from different types of moss growth forms should be collected to allow better model
377 development for moss biomass.

378 There are differences in the explanatory potential of satellite image regressions
379 across tundra or other northern landscapes with low-growth vegetation (Table 5). In a
380 comparison between two sites at Nunavut, Canada, Atkinson and Treitz (2013) got
381 higher R^2 values for their southern site which had lower average biomass and lower
382 biomass variation across plots. Also in our study, the sites with low average biomass
383 and low variation (Herschel and Tiksi) had low RMSE and high R^2_{adj} values, whereas
384 sites with high average biomass (Sodankylä and sites in NW Russia) had higher RMSE
385 and lower R^2_{adj} values. These differences could be related to within-site characteristics
386 and variation in vegetation. For instance, the relationship between NDVI (or other
387 vegetation indices) and biomass has been strong in VHSR evaluations in the Canadian
388 Arctic associated with clear NDVI gradients from non-vegetated surfaces with low
389 NDVI values to vegetated areas with high NDVI values (Atkinson and Treitz 2013;
390 Collingwood et al. 2014). Of our sites, Herschel and Tiksi had large areas with no
391 vegetation and, on the other hand, high herbaceous biomass in other places. In turn,
392 especially at the north boreal fen Sodankylä, the biomass and NDVI gradients were
393 short, and the landscape was dominated by an almost continuous moss cover. Moreover,
394 it has been shown that variation of biomass in wetter sites, such as Sodankylä in our
395 case, is not always evident in reflectance patterns as soil moisture suppresses NIR
396 reflectance (Buchhorn et al. 2013).

397 It also is noteworthy that the PFT composition differs between the study sites,
398 and this may affect the relationships between spectral reflectance and biomass.
399 Vegetation indices such as NDVI and RATIO are connected to greenness as well as

400 cellular and volume scattering by vegetation (Birth and McVey 1968; Rouse et al.
401 1973). It may be that in moss and shrub vegetation, which dominate in Sodankylä and
402 among the sites in NW Russia, biomass and reflectance variables used in our analyses
403 are not as tightly connected as in herbaceous vegetation, which has higher relative
404 biomass in Herschel and Tiksi. In shrubs, the woody part has a large contribution to
405 biomass, but they do not have as high reflectance values as leaves and other green parts
406 found in herbaceous plants. In addition, the canopy structure is different in herbs and
407 shrubs, which also affects reflectance. Furthermore, in the previous research, there have
408 been problems in estimating moss biomass with the help of spectral reflectance (Bratsch
409 et al. 2017). Especially *Sphagnum* have narrow absorption peaks in red and NIR, which
410 hampers the value of vegetation indices in biomass estimation (Bubier, Rock, and Crill
411 1997). The variation in PFTs confuse the universal relationships but are worth
412 examining in future research.

413 Examination of previous studies in sub-Arctic or Arctic environments suggests
414 that coarse patterns in vegetation and biomass distribution are easier to detect than fine-
415 scale variations. Usually moderate to high R^2_{ajd} values (>0.4) have been obtained in
416 studies from plot to circumpolar scale (Hope, Kimball, and Stow 1993; Walker et al.
417 2003; Riedel, Epstein, and Walker 2005; Heiskanen 2006; Fuchs et al. 2009; Kushida et
418 al. 2009; Reynolds et al. 2012; Atkinson and Treitz 2013; Buchhorn et al. 2013; Doiron
419 et al. 2013; Collingwood et al. 2014; Johansen and Tommervik 2014; Kushida et al.
420 2015). The highest R^2_{ajd} values (>0.7) between NDVI and biomass have been obtained
421 in studies that use moderate to coarse resolution satellite datasets (Walker et al. 2003;
422 Heiskanen 2006; Reynolds et al. 2012; Buchhorn et al. 2013; Johansen and Tommervik
423 2014; Berner et al. 2018). In studies that use plot-scale NDVI measurements or VHRS
424 imagery, the R^2_{ajd} values have often been near 0.5 or even below it (Hope, Kimball, and

425 Stow 1993; Riedel, Epstein, and Walker 2005; Fuchs et al. 2009; Kushida et al. 2009;
426 Atkinson and Treitz 2013; Kushida et al. 2015) but there are also some exceptions
427 (Atkinson and Treitz 2013; Buchhorn et al. 2013; Collingwood et al. 2014). One reason
428 behind this disparity might be that the variation in spectral reflectance patterns is more
429 evident at coarser scales, which usually also include areas with no or little biomass and
430 low NDVI values. Nevertheless, more research is needed to analyze how the biomass
431 distribution varies from fine to coarse scale across the different land cover and
432 vegetation types.

433 We showed that cross-site regressions functioned relatively well in biomass-
434 cover/height regression, with the underestimation and overestimation being relatively
435 small (Figures 3 and 4). Nevertheless, there were large potential biases and high RMSE
436 values in cross-site biomass-satellite spectra regression predictions (Figure 5, Table 6).
437 This was evident on Herschel, where there were 2–3-fold differences in the landscape-
438 scale average biomass when different regression combinations were used (Table 6).
439 This finding is in line with the study by Atkinson and Treitz (2013), who, however, had
440 only two sites at Nunavut, Canada for their comparison. The differences between sites
441 suggest that satellite image based shrub tundra models work well in different shrub
442 tundra landscapes such as NW Russian sites, but their value is limited in herbaceous
443 environments such as Herschel, and it is tedious to find suitable cross-site models.
444 Nevertheless, on Herschel, the combination of cross-site biomass-cover/height
445 regression and site-specific biomass-satellite spectra regression yielded lower RMSE
446 values than the combination of two site-specific regressions. This might be due to the
447 fact that cross-site biomass-cover/height regressions were more realistic as they had a
448 bigger sample size. Another possibility is, that although cross-site biomass-cover/height
449 regressions slightly underestimated biomass values, modelled values were such that

450 they could be modelled with satellite spectra. Nevertheless, it might be that cross-site
451 models are more robust to outliers due to larger sample size, and they can give better fit,
452 if there is no large differences in the environmental characteristics of the study sites.

453 The biomass-satellite spectra regressions that included multiple explanatory
454 variables had better prediction capability than regressions with only one index as
455 explanatory variable. Furthermore, in previous research, good explanatory power has
456 been obtained using models that combine optical imagery and other types of remote
457 sensing data both in the Arctic areas (Chen, Blain, et al. 2009; Collingwood et al. 2014;
458 Greaves et al. 2016) and other landscapes with low-growth vegetation (Glenn et al.
459 2016). In particular, features related to vegetation height, topography, moisture
460 gradients, soil properties and geomorphology could improve biomass models (Chen,
461 Blain, et al. 2009; Axmanova et al. 2012; Collingwood et al. 2014; Suvanto, Le Roux,
462 and Luoto 2014; Glenn et al. 2016; Greaves et al. 2016). In a similar manner, in
463 peatland landscapes such as Sodankylä, carbon exchange and other ecosystem
464 properties are linked to microtopographical variation (Lees et al. 2018), which could be
465 captured with VHSR digital elevation models. It may be that the benefit of other
466 datatypes is greater in areas where the relationship between reflectance and biomass is
467 weak. Therefore, future research should combine VHSR imagery with other VHSR data
468 and test what kind of models and predictor variables should be used in each kind of
469 landscape and if some predictor sets are locally optimal but not as useful in a larger
470 area.

471 Finally, our analysis did not include phenological dynamics nor did we analyze
472 the optimal timing for satellite imagery in mapping biomass distribution. Biomass and
473 other vegetation parameters change during the growing season; furthermore, the relative
474 importance of different PFTs change as the growing season proceeds (Anderson et al.

475 2016; Wang et al. 2016; Juutinen et al. 2017). It has thus been shown that the seasonal
476 phase of VHSR images affect the interpretation of vegetation parameters such as leaf-
477 area index (Juutinen et al. 2017). However, more work is needed on evaluating how the
478 timing of satellite images affects success in mapping biomass distribution.

479 **5. Conclusions**

480 We estimated aboveground biomass in four different Arctic landscapes using field
481 sampling based biomass-cover/height regressions and biomass-satellite spectra
482 regressions. We tested both site-specific regressions and cross-site regressions across all
483 the study sites, and showed that biomass-cover/height regressions perform well in most
484 cases (R^2_{adj} 0.21–0.92), and their performance varies in biomass-satellite spectra
485 regressions (R^2_{adj} 0.33–0.75). The cross-site regressions should be used with care in
486 biomass-satellite spectra regressions, as they underestimated biomass in some study
487 sites and overestimated them in other sites. However, in biomass-cover/height
488 regressions there was no large differences in predicted biomass values when site-
489 specific regressions were compared with cross-site regressions. Moreover, due to larger
490 sample size, cross-site regressions are more robust to outliers, and may yield better fit
491 than site-specific regressions when they combine data from study sites which have
492 similar vegetation and landscape characteristics. We showed that there is considerable
493 variation in biomass distribution both within and between different Arctic landscapes,
494 and the biomass and proportion of different PFTs vary between Arctic landscapes.
495 Nevertheless, there is further need for model building and validation across different
496 tundra environments, including landscape types which were not included in our study or
497 still have limited field datasets. To summarize, the usage of VHSR images creates new
498 possibilities to map the fine-scale spatial variability in biomass in landscapes with
499 patchy vegetation cover for different kind of ecosystem and modelling purposes, but

500 some caution is needed when trying to develop models performing well in different
501 environments.

502 Acknowledgments: We thank Malin Ek, Hanna Hyvönen, Maria Kröger, Maiju Linkosalmi,
503 Johanna Nyman, Tiina Ronkainen, Lauri Rosenius, Sanna Susiluoto and Emmi Vähä for field
504 and laboratory assistance. We would also like to thank the following individuals from various
505 institutes and organizations for help with different aspects and phases of field campaigns and
506 data collection: Komi Biological Institute in Syktyvkar, Tiksi Observatory and Yakutian Service
507 for Hydrometeorology, The Aurora Research Institute in Inuvik, Arctic Research Centre of
508 Finnish Meteorological Institute in Sodankylä, University of Stockholm, Alfred Wegener
509 Institute in Potsdam, University of Eastern Finland, and Natural Resources Institute Finland.
510 Data used in this study was collected in EU 6th Framework CARBONorth project [contract
511 036993], and in the following projects funded by the Academy of Finland: COUP [project
512 291736] and Greenhouse gas, aerosol and albedo variations in the changing Arctic [project
513 269095]. The paper was finalized with financial support from CAPTURE [project 296423
514 funded by the Academy of Finland].

515 **References**

- 516 AARI. 2017. "Electronic archive AARI term meteorological and upper-air observations
517 Hydrometeorological Observatory AARI 2016 (station) Tiksi for 19322014."
518 Accessed September 7. www.aari.ru/main.php?sub=2&id=3.
- 519 ———. 2017. "Electronic archive AARI term meteorological and upper-air
520 observations Hydrometeorological Observatory AARI 2016 (station) Tiksi for
521 1932 2014." Accessed September 7. www.aari.ru/main.php?sub=2&id=3.
- 522 Alexeyev, V., R. Birdsey, V. Stakanov, and I. Korotkov. 1995. "Carbon in vegetation of
523 Russian forests: Methods to estimate storage and geographical distribution."
524 *Water, Air, and Soil Pollution* 82 (1-2):271-82. doi: 10.1007/BF01182840.
- 525 Anderson, H. B., L. Nilsen, H. Tommervik, S. R. Karlsen, S. Nagai, and E. J. Cooper.
526 2016. "Using ordinary digital cameras in place of near-infrared sensors to derive
527 vegetation indices for phenology studies of high arctic vegetation." *Remote*
528 *Sensing* 8 (10). doi: 10.3390/rs8100847.
- 529 Atkinson, D. M., and P. Treitz. 2013. "Modeling biophysical variables across an Arctic
530 latitudinal gradient using high spatial resolution remote sensing data." *Arctic*
531 *Antarctic and Alpine Research* 45 (2):161-78. doi: 10.1657/1938-4246-45.2.161.
- 532 Axmanova, I., L. Tichy, Z. Fajmonova, P. Hajkova, E. Hettenbergerova, C. F. Li, K.
533 Merunkova, et al. 2012. "Estimation of herbaceous biomass from species
534 composition and cover." *Applied Vegetation Science* 15 (4):580-9. doi:
535 10.1111/j.1654-109X.2012.01191.x.
- 536 Beamish, A. L., N. C. Coops, S. Chabrilat, and B. Heim. 2017. "A Phenological
537 Approach to Spectral Differentiation of Low-Arctic Tundra Vegetation
538 Communities, North Slope, Alaska." *Remote Sensing* 9 (11):1200. doi:
539 doi:10.3390/rs9111200.

- 540 Berner, L. T., P. Jantz, K. D. Tape, and S. J. Goetz. 2018. "Tundra plant aboveground
541 biomass and shrub dominance mapped across the North Slope of Alaska."
542 *Environmental Research Letters* In press. doi: [https://doi.org/10.1088/1748-](https://doi.org/10.1088/1748-9326/aaaa9a)
543 [9326/aaaa9a](https://doi.org/10.1088/1748-9326/aaaa9a).
- 544 Birth, G. S., and G. R. McVey. 1968. "Measuring the color of growing turf with a
545 reflectance spectrophotometer." *Agronomy Journal* 60 (6):640-3. doi:
546 doi:10.2134/agronj1968.00021962006000060016x.
- 547 Bratsch, S., H. Epstein, M. Buchhorn, D. Walker, and H. Landes. 2017. "Relationships
548 between hyperspectral data and components of vegetation biomass in Low
549 Arctic tundra communities at Ivotuk, Alaska." *Environmental Research Letters*
550 12 (2). doi: 10.1088/1748-9326/aa572e.
- 551 Bubier, J. L., B. N. Rock, and P. M. Crill. 1997. "Spectral reflectance measurements of
552 boreal wetland and forest mosses." *Journal of Geophysical Research*
553 *Atmospheres* 102 (24):29483-94.
- 554 Buchhorn, M., M. K. Reynolds, and D. A. Walker. 2016. "Influence of BRDF on NDVI
555 and biomass estimations of Alaska Arctic tundra." *Environmental Research*
556 *Letters* 11 (12):125002. doi: 10.1088/1748-9326/11/12/125002.
- 557 Buchhorn, M., D. A. Walker, B. Heim, M. K. Reynolds, H. E. Epstein, and M.
558 Schwieder. 2013. "Ground-based hyperspectral characterization of Alaska
559 tundra vegetation along environmental gradients." *Remote Sensing* 5 (8):3971-
560 4005. doi: 10.3390/rs5083971.
- 561 Burn, C. R. 2012. "Climate." In *Herschel Island—Qikiqtaryuk: A Natural and Cultural*
562 *History.*, edited by C. R. Burn, 48-53. Calgary, Canada: University of Calgary
563 Press.
- 564 Chapin III, F. S., M. S. Bret-Harte, S. E. Hobbie, and H. Zhong. 1996. "Plant functional
565 types as predictors of transient responses of arctic vegetation to global change."
566 *Journal of Vegetation Science* 7 (3):347-58.
- 567 Chavez, P. S. 1988. "An improved dark-object subtraction technique for atmospheric
568 scattering correction of multispectral data." *Remote Sensing of Environment* 24
569 (3):459-79. doi: 10.1016/0034-4257(88)90019-3.
- 570 Chen, W., D. Blain, J. Li, K. Keohler, R. Fraser, Y. Zhang, S. Leblanc, I. Olthof, J.
571 Wang, and M. McGovern. 2009. "Biomass measurements and relationships with
572 Landsat-7/ETM + and JERS-1/SAR data over Canada's western sub-arctic and
573 low arctic." *International journal of remote sensing* 30 (9):2355-76. doi:
574 10.1080/01431160802549401.
- 575 Chen, W. J., J. H. Li, Y. Zhang, F. Q. Zhou, K. Koehler, S. Leblanc, R. Fraser, I.
576 Olthof, Y. S. Zhang, and J. X. Wang. 2009. "Relating biomass and leaf area
577 index to non-destructive measurements in order to monitor changes in arctic
578 vegetation." *Arctic* 62 (3):281-94.
- 579 Collingwood, A., P. Treitz, F. Charbonneau, and D. M. Atkinson. 2014. "Artificial
580 neural network modeling of high arctic phytomass using synthetic aperture radar
581 and multispectral data." *Remote Sensing* 6 (3):2134-53. doi:
582 10.3390/rs6032134.
- 583 Coops, N. C., M. Johnson, M. A. Wulder, and J. C. White. 2006. "Assessment of
584 QuickBird high spatial resolution imagery to detect red attack damage due to
585 mountain pine beetle infestation." *Remote Sensing of Environment* 103 (1):67-
586 80. doi: 10.1016/j.rse.2006.03.012.
- 587 Dinsmore, K. J., J. Drewer, P. E. Levy, C. George, A. Lohila, M. Aurela, and U. M.
588 Skiba. 2017. "Growing season CH₄ and N₂O fluxes from a subarctic landscape

- 589 in northern Finland; From chamber to landscape scale." *Biogeosciences* 14
590 (4):799-815. doi: 10.5194/bg-14-799-2017.
- 591 Doiron, M., P. Legagneux, G. Gauthier, and E. Levesque. 2013. "Broad-scale satellite
592 Normalized Difference Vegetation Index data predict plant biomass and peak
593 date of nitrogen concentration in Arctic tundra vegetation." *Applied Vegetation
594 Science* 16 (2):343-51. doi: 10.1111/j.1654-109X.2012.01219.x.
- 595 Eckert, S. 2012. "Improved forest biomass and carbon estimations using texture
596 measures from worldView-2 satellite data." *Remote Sensing* 4 (4):810-29. doi:
597 10.3390/rs4040810.
- 598 Epstein, H. E., M. K. Raynolds, D. A. Walker, U. S. Bhatt, C. J. Tucker, and J. E.
599 Pinzon. 2012. "Dynamics of aboveground phytomass of the circumpolar Arctic
600 tundra during the past three decades." *Environmental Research Letters* 7 (1).
601 doi: 10.1088/1748-9326/7/1/015506.
- 602 Finnish Meteorological Institute. 2017. "July statistics." Accessed September 9.
603 <http://ilmatieteenlaitos.fi/heinakuu>.
- 604 Fox, J., and S. Weisberg. 2011. *An {R} Companion to Applied Regression, Second
605 Edition*. Thousand Oaks, CA, USA: Sage.
- 606 Fuchs, H., P. Magdon, C. Kleinn, and H. Flessa. 2009. "Estimating aboveground carbon
607 in a catchment of the Siberian forest tundra: Combining satellite imagery and
608 field inventory." *Remote Sensing of Environment* 113 (3):518-31. doi:
609 10.1016/j.rse.2008.07.017.
- 610 Glenn, N. F., A. Neuenschwander, L. A. Vierling, L. Spaete, A. Li, D. J. Shinneman, D.
611 S. Pilliod, R. S. Arkle, and S. K. McIlroy. 2016. "Landsat 8 and ICESat-2:
612 Performance and potential synergies for quantifying dryland ecosystem
613 vegetation cover and biomass." *Remote Sensing of Environment* 185:233-42.
614 doi: 10.1016/j.rse.2016.02.039.
- 615 Greaves, H. E., L. A. Vierling, J. U. H. Eitel, N. T. Boelman, T. S. Magney, C. M.
616 Prager, and K. L. Griffin. 2016. "High-resolution mapping of aboveground
617 shrub biomass in Arctic tundra using airborne lidar and imagery." *Remote
618 Sensing of Environment* 184:361-73. doi: 10.1016/j.rse.2016.07.026.
- 619 Grosswald, M. G., W. Karlen, Z. Shishorina, and A. Bodin. 1992. "Glacial landforms
620 and the age of deglaciation in the Tiksi area, east Siberia." *Geografiska
621 Annaler, Series A* 74 A (4):295-304.
- 622 Heiskanen, J. 2006. "Estimating aboveground tree biomass and leaf area index in a
623 mountain birch forest using ASTER satellite data." *International journal of
624 remote sensing* 27 (5-6):1135-58. doi: 10.1080/01431160500353858.
- 625 Hope, A. S., J. S. Kimball, and D. A. Stow. 1993. "The relationship between tussock
626 tundra spectral reflectance properties and biomass and vegetation composition."
627 *International journal of remote sensing* 14 (10):1861-74.
- 628 Huete, A. R. 1988. "A soil-adjusted vegetation index (SAVI)." *Remote Sensing of
629 Environment* 25 (3):295-309. doi: 10.1016/0034-4257(88)90106-x.
- 630 Hugelius, G., T. Virtanen, D. Kaverin, A. Pastukhov, F. Rivkin, S. Marchenko, V.
631 Romanovsky, and P. Kuhry. 2011. "High-resolution mapping of ecosystem
632 carbon storage and potential effects of permafrost thaw in periglacial terrain,
633 European Russian Arctic." *Journal of Geophysical Research: Biogeosciences*
634 116 (3). doi: 10.1029/2010JG001606.
- 635 Jiang, Z. Y., A. R. Huete, K. Didan, and T. Miura. 2008. "Development of a two-band
636 enhanced vegetation index without a blue band." *Remote Sensing of
637 Environment* 112 (10):3833-45. doi: 10.1016/j.rse.2008.06.006.

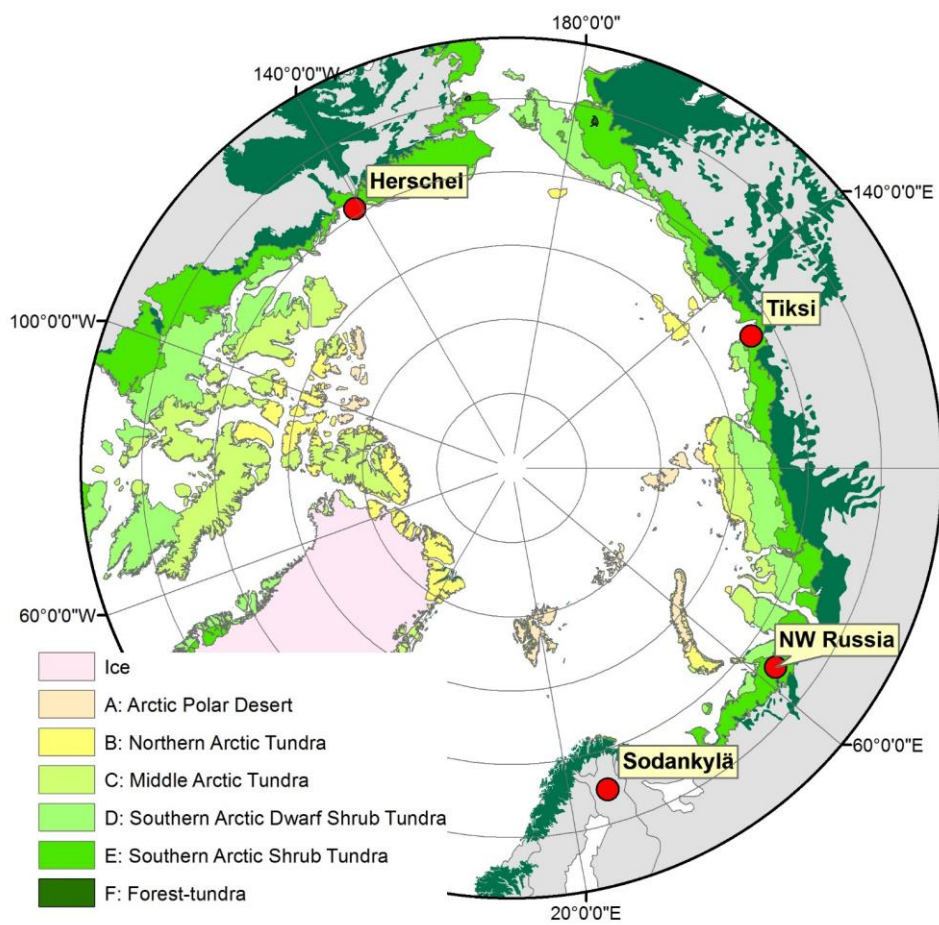
- 638 Johansen, B., and H. Tommervik. 2014. "The relationship between phytomass, NDVI
639 and vegetation communities Svalbard." *International Journal of Applied Earth*
640 *Observation and Geoinformation* 27:20-30. doi: 10.1016/j.jag.2013.07.001.
- 641 Juutinen, S., T. Virtanen, V. Kondratyev, T. Laurila, M. Linkosalmi, J. Mikola, J.
642 Nyman, A. Räsänen, J-P. Tuovinen, and M. Aurela. 2017. "Spatial variation and
643 seasonal dynamics of leaf-area index in the arctic tundra-implications for linking
644 ground observations and satellite images." *Environmental Research Letters*
645 12:095002. doi: <https://doi.org/10.1088/1748-9326/aa7f85>.
- 646 Kauppi, P. E., E. Tomppo, and A. Ferm. 1995. "C and N storage in living trees within
647 Finland since 1950s." *Plant and Soil* 168-169 (1):633-8. doi:
648 10.1007/BF00029377.
- 649 Korpela, I. 2001. "Metsänarviointi. Luentomoniste teknillisen korkeakoulun
650 metsänarvioinnin kurssille." In. Helsinki, Finland: University of Helsinki.
- 651 Kuhn, M., J. Wing, S. Weston, A. Williams, C. Keefer, A. Engelhardt, T. Cooper, et al.
652 "caret: classification and regression training. R package version 6.0-71."
653 <http://CRAN.R-project.org/package=caret>.
- 654 Kushida, K., S. Hobara, S. Tsuyuzaki, Y. Kim, M. Watanabe, Y. Setiawan, K. Harada,
655 G. R. Shaver, and M. Fukuda. 2015. "Spectral indices for remote sensing of
656 phytomass, deciduous shrubs, and productivity in Alaskan Arctic tundra."
657 *International journal of remote sensing* 36 (17):4344-62. doi:
658 10.1080/01431161.2015.1080878.
- 659 Kushida, K., Y. Kim, S. Tsuyuzaki, and M. Fukuda. 2009. "Spectral vegetation indices
660 for estimating shrub cover, green phytomass and leaf turnover in a sedge-shrub
661 tundra." *International journal of remote sensing* 30 (6):1651-8. doi:
662 10.1080/01431160802502632.
- 663 Laidler, G. J., and P. Treitz. 2003. "Biophysical remote sensing of arctic environments."
664 *Progress in Physical Geography* 27 (1):44-68. doi:
665 10.1191/0309133303pp358ra.
- 666 Lees, K. J., T. Quaife, R. R. E. Artz, M. Khomik, and J. M. Clark. 2018. "Potential for
667 using remote sensing to estimate carbon fluxes across northern peatlands – A
668 review." *Science of the Total Environment* 615:857-74. doi:
669 10.1016/j.scitotenv.2017.09.103.
- 670 Liu, H. Q., and A. Huete. 1995. "A feedback based modification of the NDVI to
671 minimize canopy background and atmospheric noise." *Ieee Transactions on*
672 *Geoscience and Remote Sensing* 33 (2):457-65.
- 673 Marushchak, M. E., I. Kiepe, C. Biasi, V. Elsakov, T. Friborg, T. Johansson, H.
674 Soegaard, T. Virtanen, and P. J. Martikainen. 2013. "Carbon dioxide balance of
675 subarctic tundra from plot to regional scales." *Biogeosciences* 10 (1):437-52.
676 doi: 10.5194/bg-10-437-2013.
- 677 McDonald, J.H. 2014. *Handbook of Biological Statistics*. 3rd ed. ed. Baltimore,
678 Maryland, USA: Sparky House Publishing.
- 679 Mikola, J., T. Virtanen, M. Linkosalmi, E. Vähä, J. Nyman, O. Postanogova, A.
680 Räsänen, et al. 2018. "Spatial variation and linkages of soil and vegetation in the
681 Siberian Arctic tundra - Coupling field observations with remote sensing data."
682 *Biogeosciences* 15 (9):2781-801. doi: 10.5194/bg-15-2781-2018.
- 683 Myers-Smith, I. H., S. C. Elmendorf, P. S. A. Beck, M. Wilmking, M. Hallinger, D.
684 Blok, K. D. Tape, et al. 2015. "Climate sensitivity of shrub growth across the
685 tundra biome." *Nature Climate Change* 5 (9):887-+. doi: 10.1038/nclimate2697.
- 686 Myers-Smith, I. H., D. S. Hik, C. Kennedy, D. Cooley, J. F. Johnstone, A. J. Kenney,
687 and C. J. Krebs. 2011. "Expansion of canopy-forming willows over the

- 688 twentieth century on Herschel Island, Yukon Territory, Canada." *Ambio* 40
689 (6):610-23. doi: 10.1007/s13280-011-0168-y.
- 690 Nyyssönen, A. 1955. "Metsikön kuutiomäärän arvioiminen relaskoopin avulla."
691 *Metsäntutkimuslaitoksen julkaisuja* 44 (6):1-31.
- 692 Obu, J., H. Lantuit, I. Myers-Smith, B. Heim, J. Wolter, and M. Fritz. 2017. "Effect of
693 terrain characteristics on soil organic carbon and total nitrogen stocks in soils of
694 Herschel Island, western Canadian Arctic." *Permafrost and Periglacial*
695 *Processes* 28 (1):92-107. doi: 10.1002/ppp.1881.
- 696 Qi, J., A. Chehbouni, A. R. Huete, Y. H. Kerr, and S. Sorooshian. 1994. "A modified
697 soil adjusted vegetation index." *Remote Sensing of Environment* 48 (2):119-26.
698 doi: 10.1016/0034-4257(94)90134-1.
- 699 R Core Team. "R: A language and environment for statistical computing." R
700 Foundation for Statistical Computing. <https://www.R-project.org/>.
- 701 Reynolds, M. K., D. A. Walker, H. E. Epstein, J. E. Pinzon, and C. J. Tucker. 2012. "A
702 new estimate of tundra-biome phytomass from trans-Arctic field data and
703 AVHRR NDVI." *Remote Sensing Letters* 3 (5):403-11. doi:
704 10.1080/01431161.2011.609188.
- 705 Reynolds, M. K., D. A. Walker, and H. A. Maier. 2006. "NDVI patterns and phytomass
706 distribution in the circumpolar Arctic." *Remote Sensing of Environment* 102 (3-
707 4):271-81. doi: 10.1016/j.rse.2006.02.016.
- 708 Riedel, S. M., H. E. Epstein, and D. A. Walker. 2005. "Biotic controls over spectral
709 reflectance of arctic tundra vegetation." *International journal of remote sensing*
710 26 (11):2391-405. doi: 10.1080/01431160512331337754.
- 711 Rouse, J. W. Jr., R. H. Haas, J. A. Schell, and D. W. Deering. 1973. "Monitoring
712 vegetation systems in the Great Plains with ERTS." In *Third Earth Resources*
713 *Technology Satellite-1 Symposium*, 309-17. Washington, DC: NASA.
- 714 Shepashenko, D., A. Shvidenko, and S. Nilsson. 1998. "Phytomass (live biomass) and
715 carbon of Siberian forests." *Biomass & Bioenergy* 14 (1):21-31. doi:
716 10.1016/s0961-9534(97)10006-x.
- 717 Siewert, M. B., J. Hanisch, N. Weiss, P. Kuhry, T. C. Maximov, and G. Hugelius. 2015.
718 "Comparing carbon storage of Siberian tundra and taiga permafrost ecosystems
719 at very high spatial resolution." *Journal of Geophysical Research-*
720 *Biogeosciences* 120 (10):1973-94. doi: 10.1002/2015jg002999.
- 721 Sinha, S., C. Jeganathan, L. K. Sharma, and M. S. Nathawat. 2015. "A review of radar
722 remote sensing for biomass estimation." *International Journal of Environmental*
723 *Science and Technology* 12 (5):1779-92. doi: 10.1007/s13762-015-0750-0.
- 724 Smith, C. A. S., C. E. Kennedy, A. E. Hargrave, and McKenna K. M. 1989. *Soil and*
725 *vegetation survey of Herschel Island, Yukon Territory., Yukon Soil Survey*
726 *Report, No. 1. LRRC Contribution No. 88-26.* Whitehorse Yukon: Agriculture
727 Canada.
- 728 Song, C., C. E. Woodcock, K. C. Seto, M. P. Lenney, and S. A. Macomber. 2001.
729 "Classification and change detection using Landsat TM data: When and how to
730 correct atmospheric effects?" *Remote Sensing of Environment* 75 (2):230-44.
731 doi: 10.1016/s0034-4257(00)00169-3.
- 732 Starr, M., M. Hartman, and T. Kinnunen. 1998. "Biomass functions for mountain birch
733 in the Vuoskojärvi Integrated Monitoring area." *Boreal Environment Research*
734 3 (3):297-303.
- 735 Steele-Dunne, S. C., H. McNairn, A. Monsivais-Huertero, J. Judge, P. W. Liu, and K.
736 Papathanassiou. 2017. "Radar remote sensing of agricultural canopies: A

- 737 Review." *Ieee Journal of Selected Topics in Applied Earth Observations and*
738 *Remote Sensing* 10 (5):2249-73. doi: 10.1109/JSTARS.2016.2639043.
- 739 Stow, D. A., A. Hope, D. McGuire, D. Verbyla, J. Gamon, F. Huemmrich, S. Houston,
740 et al. 2004. "Remote sensing of vegetation and land-cover change in Arctic
741 Tundra Ecosystems." *Remote Sensing of Environment* 89 (3):281-308. doi:
742 10.1016/j.rse.2003.10.018.
- 743 Suvanto, S., P. C. Le Roux, and M. Luoto. 2014. "Arctic-alpine vegetation biomass is
744 driven by fine-scale abiotic heterogeneity." *Geografiska Annaler Series a-*
745 *Physical Geography* 96 (4):549-60. doi: 10.1111/geoa.12050.
- 746 Walker, D. A., F. J. A. Daniëls, I. Alsos, U. S. Bhatt, A. L. Breen, M. Buchhorn, H.
747 Bültmann, et al. 2016. "Circumpolar Arctic vegetation: A hierarchic review and
748 roadmap toward an internationally consistent approach to survey, archive and
749 classify tundra plot data." *Environmental Research Letters* 11 (5). doi:
750 10.1088/1748-9326/11/5/055005.
- 751 Walker, D. A., H. E. Epstein, G. J. Jia, A. Balsler, C. Copass, E. J. Edwards, W. A.
752 Gould, et al. 2003. "Phytomass, LAI, and NDVI in northern Alaska:
753 Relationships to summer warmth, soil pH, plant functional types, and
754 extrapolation to the circumpolar Arctic." *Journal of Geophysical Research-*
755 *Atmospheres* 108 (D2). doi: 10.1029/2001jd000986.
- 756 van der Wal, R., and A. Stien. 2014. "High-arctic plants like it hot: a long-term
757 investigation of between-year variability in plant biomass." *Ecology* 95
758 (12):3414-27.
- 759 Wang, P., L. Mommer, J. van Ruijven, F. Berendse, T. C. Maximov, and Mmpd
760 Heijmans. 2016. "Seasonal changes and vertical distribution of root standing
761 biomass of graminoids and shrubs at a Siberian tundra site." *Plant and Soil* 407
762 (1-2):55-65. doi: 10.1007/s11104-016-2858-5.
- 763 Varmola, M., and E. Vuokila. 1986. "Pienten mäntyjen tilavuusyhtälöt ja -taulukot. Tree
764 volume functions and tables for small-sized pines." In *Folia Forestalia* 652, 24.
765 Helsinki, Finland: The Finnish Forest Research Institute.
- 766 Venables, W. N., and B. D. Ripley. 2003. *Modern Applied Statistics with S. Fourth*
767 *Edition*. New York, NY, USA: Springer.
- 768 Westergaard-Nielsen, A., A. B. Bjørnsson, M. R. Jepsen, M. Stendel, B. U. Hansen, and
769 B. Elberling. 2015. "Greenlandic sheep farming controlled by vegetation
770 response today and at the end of the 21st Century." *Science of the Total*
771 *Environment* 512-513:672-81. doi: 10.1016/j.scitotenv.2015.01.039.
- 772 Westergaard-Nielsen, A., M. Lund, B. U. Hansen, and M. P. Tamstorf. 2013. "Camera
773 derived vegetation greenness index as proxy for gross primary production in a
774 low Arctic wetland area." *ISPRS Journal of Photogrammetry and Remote*
775 *Sensing* 86:89-99. doi: 10.1016/j.isprsjprs.2013.09.006.
- 776 Virtanen, T., and M. Ek. 2014. "The fragmented nature of tundra landscape."
777 *International Journal of Applied Earth Observation and Geoinformation* 27:4-
778 12. doi: 10.1016/j.jag.2013.05.010.

779

780



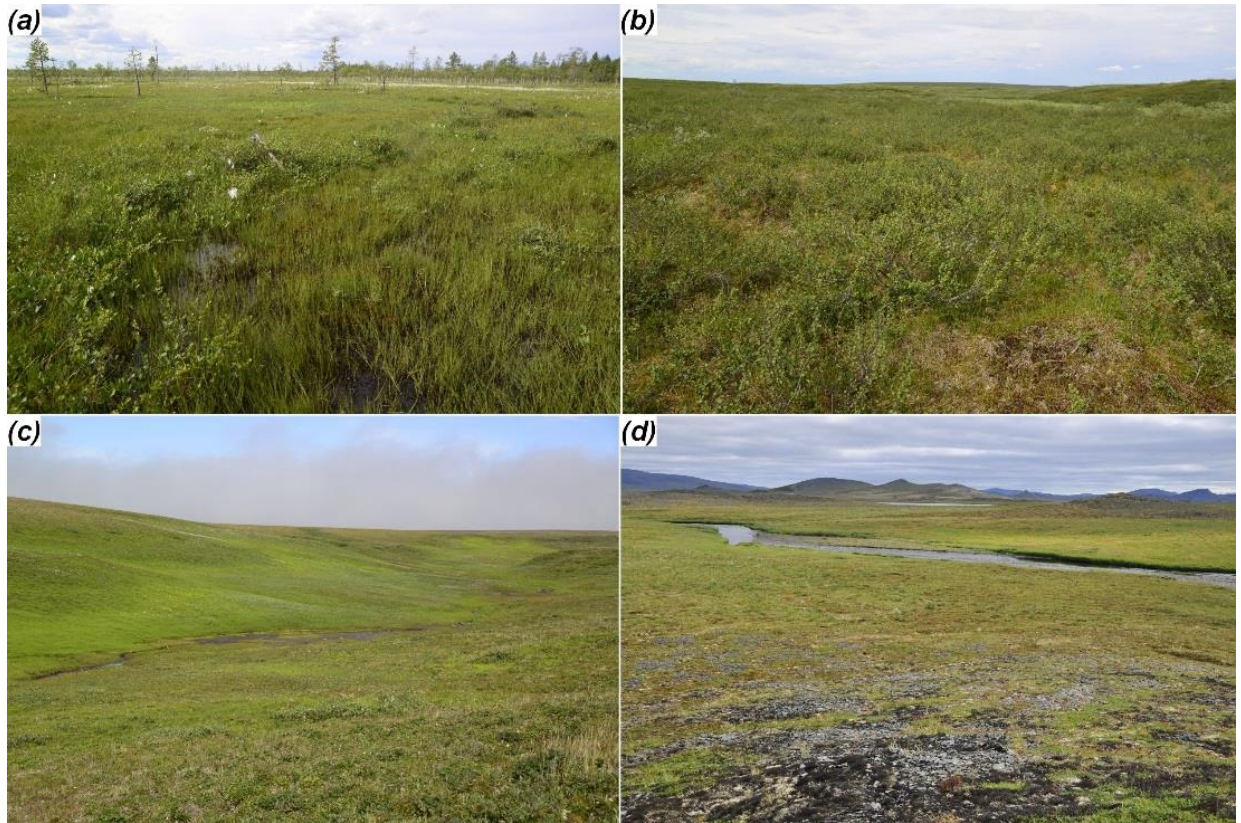
781

782 Figure 1. Location of the study sites. Vegetation zones A–E are based on Walker et al.

783 (2005) and forest tundra (F) on Olson et al. (2001). Sodankylä belongs to the northern

784 boreal vegetation zone.

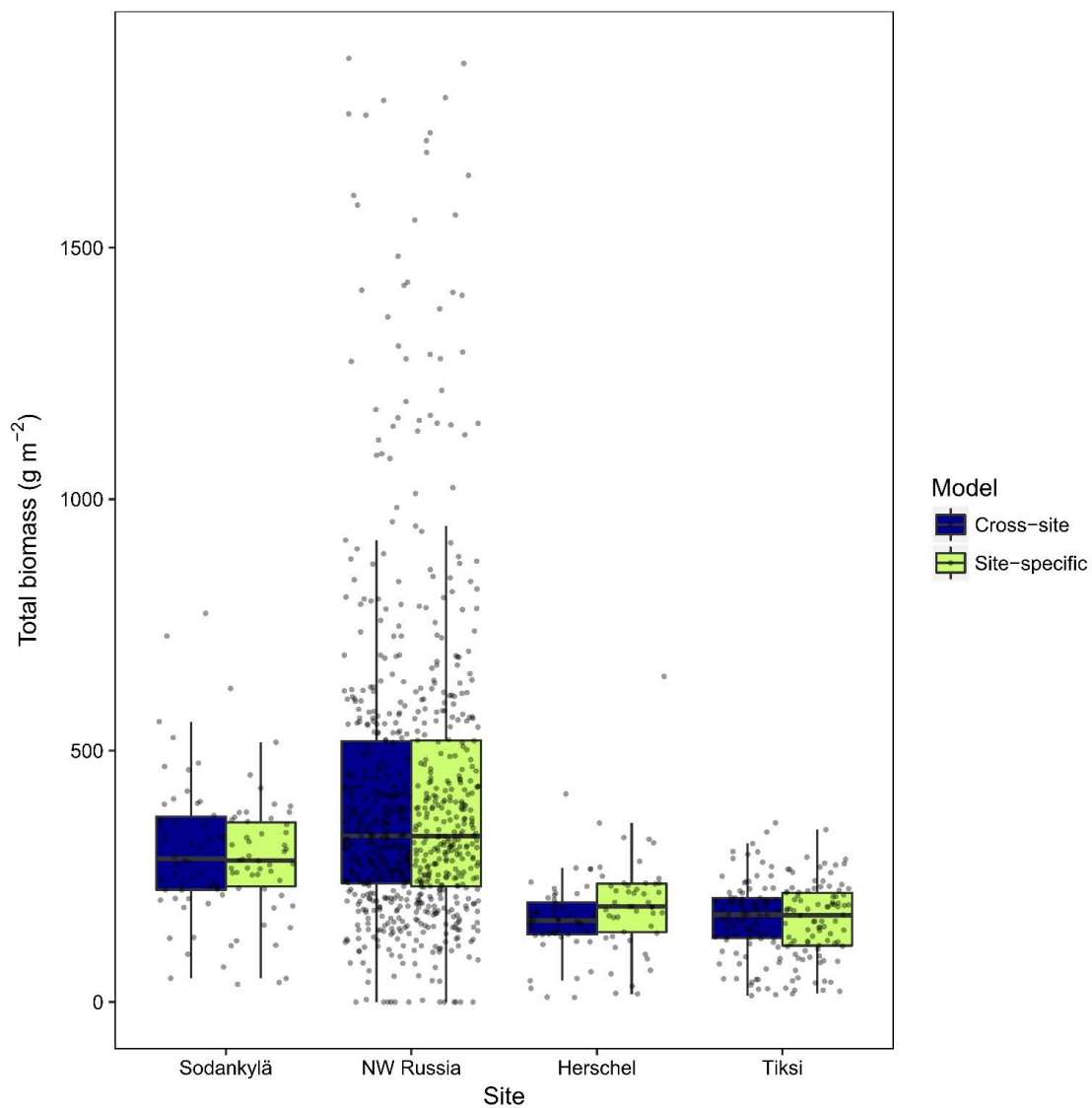
785



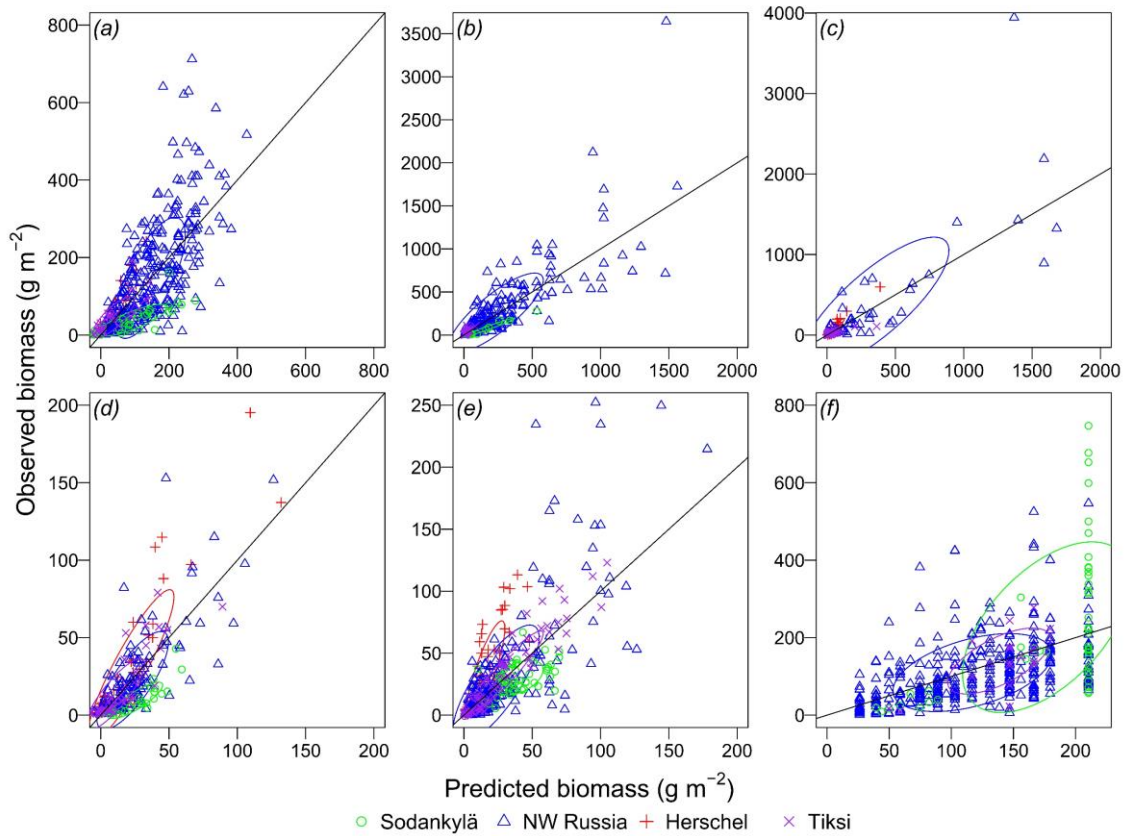
786

787 Figure 2. Study sites (a) Sodankylä, (b) Seida in Northwestern Russia, (c) Herschel

788 Island, and (d) Tiksi.

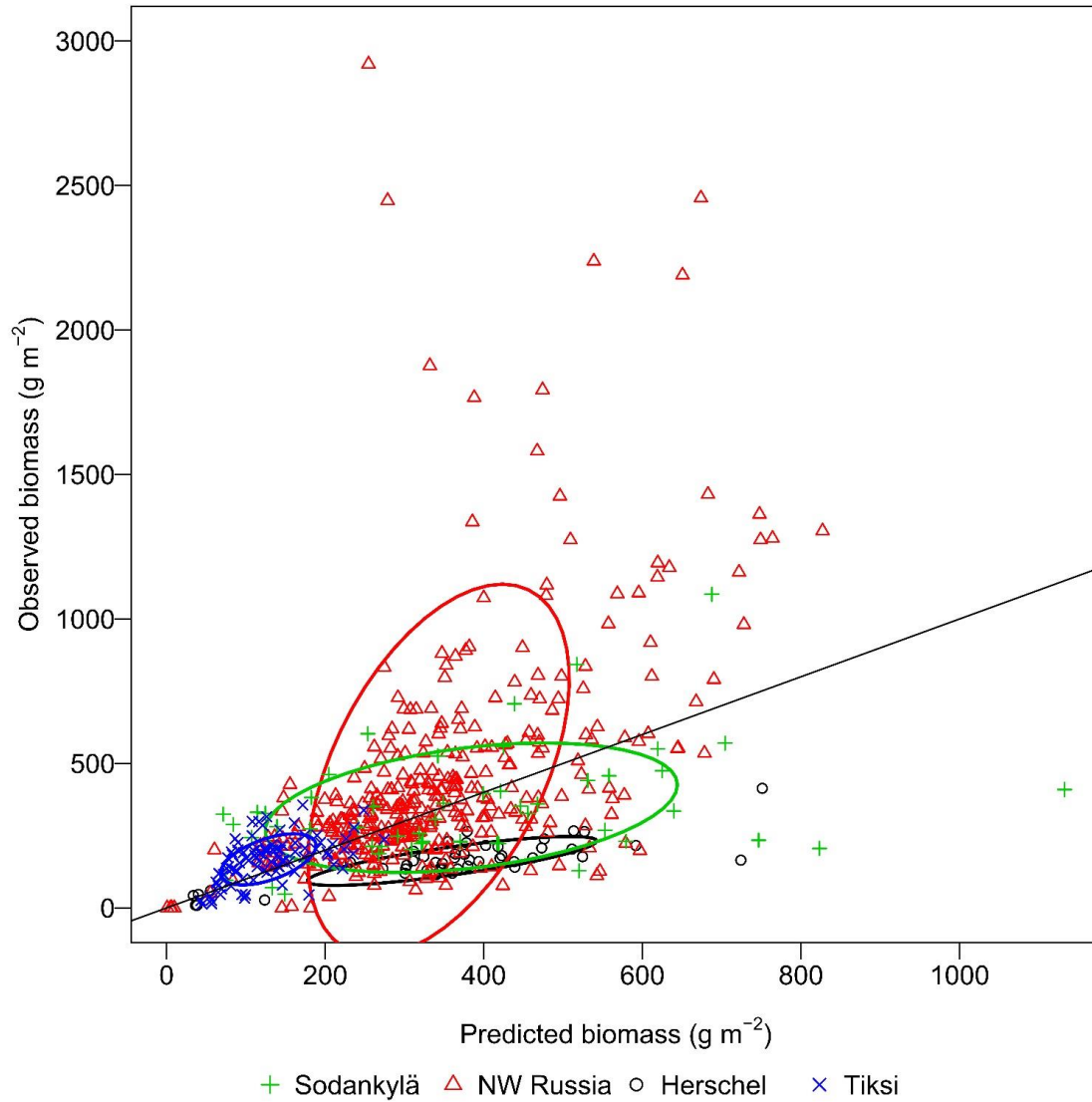


789
 790 Figure 3. Distribution of total aboveground biomass estimated for 5 m radius plots at each
 791 study site using cross-site and site-specific regressions. Note: Sodankylä and NW Russia
 792 estimates do not include tree biomass. Lines in the middle of the boxes show the median
 793 value and the lower and upper hinges are the first and third quartiles. The lower and upper
 794 whiskers extend to the smallest and largest values which are no further than 1.5 times the
 795 distance between the first and third quartiles.



796

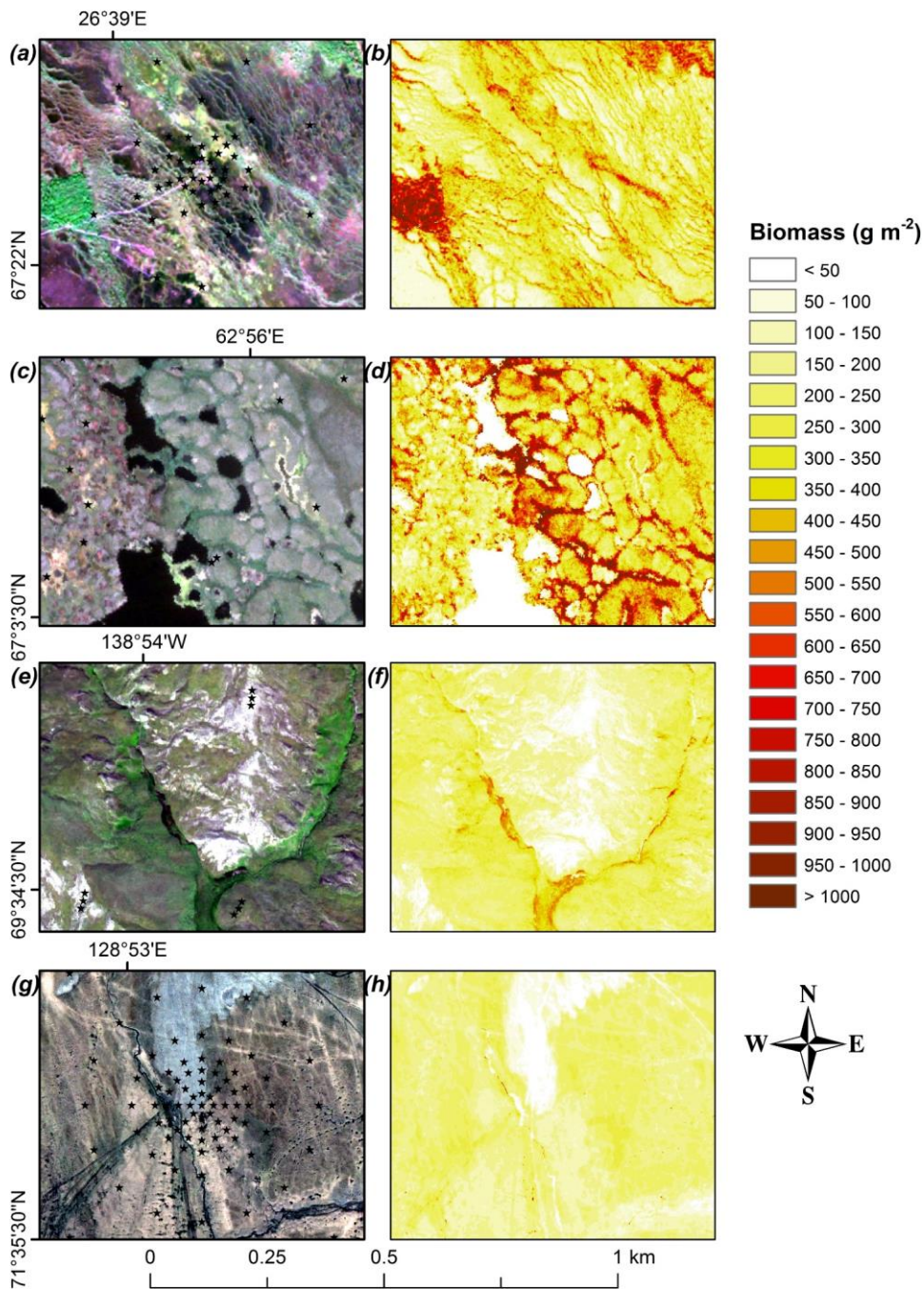
797 Figure 4. Observed (y-axis) vs. predicted i.e. harvested (x-axis) biomass for harvested
 798 plots (symbols) for (a) dwarf shrubs, (b) *Betula nana*, (c) *Salix* spp., (d) herbs, (e)
 799 graminoids and (f) mosses. Cross-site regressions for different plant functional groups
 800 were applied and the 1:1 line is shown. For each study site, individual plots are marked
 801 with symbols and the 50% confidence interval with an ellipsoid.



802

803 Figure 5. Predicted biomass (x-axis) against observed biomass in the best fitting cross-
 804 site biomass- satellite spectra regression. Observed biomass is the sum of the predicted
 805 values of the best fitting cross-site biomass-cover/height regressions for each PFT and
 806 tree biomass. For each study site, individual plots are marked with asterisks and a 50%
 807 confidence interval with an ellipsoid. Line represents a 1:1 line. To increase readability
 808 of the plot, three observations with > 3000 g m⁻² observed biomass were removed from
 809 the plot.

810



811

812 Figure 6. RGB satellite images and biomass maps for Sodankylä (a, b), Seida in NW
 813 Russia (c, d), Herschel (e, f), and Tiksi (g, h). Biomass maps were produced with the
 814 best fitting site-specific regressions (see Table 5). Spatial resolution of the images is
 815 shown in Table 1 and biomass maps have same pixel size as the images. In the satellite
 816 images, the location of the field sampling plots are shown with star symbols. For
 817 Seida/NW Russia and Herschel, only part of the field sampling plots are shown, because
 818 the plots were collected from a larger area. Satellite images ©Digital Globe.

819

820 Table 1. Coordinates of the study sites, mean July temperature sensor and imagery
 821 information, and date of the field data collection. In the column “Sensor”, WV refers to
 822 WorldView and QB to QuickBird.

Study site	Location	Mean July temperature (°C)	Sensor	Pixel size (m)	Imagery date	Fieldwork date	Number of plots
Sodankylä	67° 22' N 26° 39' E	14.5 ¹	WV-2	2	4 July 2015	15–20 July 2014	50
Khosedayu ²	67° 3' N 59° 25' E	13 ³	QB	2.4	30 June 2008	19–25 July 2007	60
Seida ²	67° 4' N 62° 56' E	13 ³	QB	2.4	6 July 2007	5 July–6 Aug 2007 24–27 July 2016	150 ⁴ 32
Rogovaya 1 ²	67° 22' N 62° 15' E	13 ³	QB	2.4	4 July 2007	8–11 July 2007	62
Rogovaya 2 ²	67° 17' N 62° 6' E	13 ³	QB	2.4	4 July 2007	13–17 July 2007	62
Herschel	69° 35' N 138° 55' W	9 ⁵	WV-3	1.6	8 Aug 2015	23 July–3 Aug 2015	48
Tiksi	71° 35' N 128° 53' E	7 ⁶	QB	0.6 ⁷	15 July 2005	23–27 July 2014	91

823 ¹(Finnish Meteorological Institute 2017)

824 ²Analyzed together with other northwestern (NW) Russia study sites (Khosedayu, Seida, Rogovaya 1 and
 825 2).

826 ³(Marushchak et al. 2013)

827 ⁴In addition, we used data from 34 extra subplots in biomass-cover/height regressions.

828 ⁵(Burn 2012)

829 ⁶(AARI 2017b)

830 ⁷Image was delivered as a pan-sharpened product, i.e. all multispectral bands had 0.6 m resolution.

831

832

833 Table 2. Calculated vegetation indices, their references, and equations. Variables in the
 834 table refer to the respective spectral bands of the images and NIR to near infrared.
 835 Normalized difference vegetation index 2 was calculated only for WorldView images as
 836 it includes the near infrared 2 (NIR2) band.

Index	Equation
Normalized difference vegetation index (NDVI) (Rouse et al. 1973)	$NDVI = \frac{((NIR) - (red))}{((NIR) + (red))}$
Normalized difference vegetation index 2 (NDVI2) (Eckert 2012)	$NDVI2 = \frac{((NIR2) - (red))}{((NIR2) + (red))}$
Red-green index (RGI) (Coops et al. 2006)	$RGI = \frac{((green) - (red))}{((green) + (red))}$
Simple ratio (RATIO) (Birth and McVey 1968)	$RATIO = \frac{(red)}{(NIR)}$
Enhanced vegetation index (EVI) (Liu and Huete 1995)	$EVI = 2.5 \times \frac{((NIR) - (red))}{((NIR) + 6 \times (red) - 7.5 \times (blue) + 1)}$
Enhanced vegetation index 2 (EVI2) (Jiang et al. 2008)	$EVI2 = 2.5 \times \frac{((NIR) - (red))}{((NIR) + 2.4 \times (red) + 1)}$
Soil-adjusted vegetation index (SAVI) (Huete 1988)	$SAVI = \frac{((NIR) - (red))}{((NIR) + (red) + 1)} \times 1.5$
Modified SAVI (MSAVI2) (Qi et al. 1994)	$MSAVI2 = \frac{(2 \times (NIR) + 1 - \sqrt{(2 \times (NIR) + 1)^2 - 8 \times ((NIR) - (red))})}{2}$

837

838 Table 3. Average \pm standard deviation of biomass values for each plant functional type
 839 and study site based on field samples. The plant functional type with highest biomass at
 840 each site is shown in bold. Note: moss biomass for Herschel and Tiksi and tree biomass
 841 are not included in this table.

Study site	Biomass (g m ⁻²)						
	Dwarf shrubs	<i>B. nana</i>	<i>Salix</i> spp.	Herbs	Graminoid s	Mosses	Total
						217.9±187.	
Sodankylä	27.9±33	16.5±51.9	0.5±8.4	5.4±8.7	30.3±11.8	6	298.4±210
NW		157.3±329.	46.4±270.				439.3±431.
Russia	114.7±132.0	3	5	7.9±19.1	18.7±36.8	102.9±87.0	6
				28.8±40.			178.8±116.
Herschel	37.2±54.2	12.2±61.2	65.1±98.1	0	35.5±32.7	-	1
Tiksi	15.1±32.6	10.4±22.3	16.9±24.2	8.8±16.7	28.2±30	-	79.4±46.9

842

843

844 Table 4. Equations for different biomass-cover/height regressions for predicting plant
 845 functional type biomass (bm). Adjusted coefficient of determination (R^2_{adj}) values,
 846 average biomass in the training data (harvested data), root mean square error (RMSE)
 847 values, and p -values are also given. In the table, c refers to %-cover and h to height.

Plant functional group	Site	Equation	R^2_{adj}	Average biomass (g m ⁻²)	RMSE (g m ⁻²)	p -value
Dwarf shrubs	Cross-site	$bm = -31.85+2.98xc+8.01xh$	0.52	121.6	86.9	< 0.0001
	Sodankylä	$bm = -15.12+90.46xasin(c)+1.58xh$	0.65	35.7	19.3	< 0.0001
	NW Russia	$bm = -186.89+265.36xasin(c)+61.06x\sqrt{h}$	0.50	146.6	92.9	< 0.0001
	Herschel	$bm = -0.86+19.75xasin(c)$	0.87	61.2	18.9	< 0.0001
	Tiksi	$bm = -46.83+136.72xasin(c)+26.56x\sqrt{h}$	0.61	40.4	26.2	< 0.0001
<i>Betula nana</i>	Cross-site	$\sqrt{bm} = 1.05+0.22xc+ 0.22xh$	0.79	226.7	212.4	< 0.0001
	Sodankylä	$\sqrt{bm} = -0.38+0.22xc+0.11xh$	0.92	74.8	16.4	< 0.0001
	NW Russia	$\sqrt{bm} = -5.07+0.22xc+ 2.56x\sqrt{h}$	0.79	256.9	224.7	< 0.0001
	Herschel	n.a.	-	-	-	-
	Tiksi	$bm = 1.37+3.30xc$	0.62	30.6	17.4	< 0.0001
<i>Salix</i> spp.	Cross-site	$\sqrt{bm} = 0.88+ 0.28xc+0.13xh$	0.78	154.8	252.4	< 0.0001
	Sodankylä	n.a.	-	-	-	-
	NW Russia	$\sqrt{bm} = -0.36+0.30xc+0.14xh$	0.72	403.2	424.4	< 0.0001
	Herschel	$\sqrt{bm} = -0.09x0.40xc+0.15xh$	0.83	77.3	30.2	< 0.0001
	Tiksi	$bm = 0.95+1.97xc$	0.84	25.2	10.3	< 0.0001
Herbs	Cross-site	$bm = -8.46+94.21xasin(c)-3.24xln(h)$	0.63	20.2	17.1	< 0.0001
	Sodankylä	$\sqrt{bm} = 0.41+0.10xc+0.05xh$	0.83	9.3	4.1	< 0.0001
	NW Russia	$bm = -20.75+80.38xasin(c)+3.95xln(h)$	0.63	22.2	16.2	< 0.0001
	Herschel	$bm = -0.02+1.78xc+0.85xln(h)$	0.84	31.3	16.0	< 0.0001
	Tiksi	$bm = 1.15+86.58xasin(c)-6.67xln(h)$	0.73	12.6	9.9	< 0.0001
Graminoids	Cross-site	$\sqrt{bm} = -2.06+6.53xasin(c)+1.08\sqrt{h}$	0.64	27.9	23.8	< 0.0001
	Sodankylä	$bm = 20.62+0.46xc-0.29xh$	0.24	30.3	9.9	0.0005
	NW Russia	$\sqrt{bm} = -2.48+7.04xasin(c)+1.07x\sqrt{h}$	0.66	25.3	25.5	< 0.0001
	Herschel	$\sqrt{bm} = -4.58+12.48xasin(c)+2.36xln(h)$	0.77	36.9	16.8	< 0.0001
	Tiksi	$bm = -5.71+1.23xc+0.89xh$	0.89	31.6	9.8	< 0.0001
Mosses	Cross-site	$bm = -4.71+136.97xasin(c)$	0.28	124.9	91.7	< 0.0001
	Sodankylä	$bm = -96.01+244.10xasin(c)$	0.28	227.0	154.2	< 0.0001
	NW Russia	$bm = 20.72+100.37xasin(c)$	0.21	110.1	75.5	< 0.0001
	Herschel	n.a.	-	-	-	-
	Tiksi	$bm = -49.06+180.46xasin(c)$	0.38	139.7	52.9	0.0022

848

849

850 Table 5. Regression equations, adjusted coefficient of determination (R^2_{adj}) values, and
 851 p -values for biomass-satellite spectra regressions. For all sites, the results are shown for
 852 regressions with the lowest root mean square error value using both site-specific and
 853 cross-site height-cover based biomass estimations. In the table, bm refers to
 854 aboveground biomass.

Site	Cover/height-based estimation	Best regression	R^2_{adj}	p -value
Cross-site Sodankylä	Cross-site	$\ln(\text{bm}) = 3.84 + 31.19 \times \text{SAVI} + 13.02 \times \text{RED} - 23.54 \times \text{NIR}$	0.47	< 0.0001
	Cross-site	$\ln(\text{bm}) = 5.73 - 12.03 \times \text{RATIO} + 135.53 \times \text{COASTAL} - 13.39 \times \text{GREEN}$	0.33	< 0.0001
NW Russia	Site-specific	$\ln(\text{bm}) = 6.01 - 11.17 \times \text{RATIO} + 77.93 \times \text{COASTAL}$	0.33	< 0.0001
	Cross-site	$\ln(\text{bm}) = 8.32 - 8.35 \times \text{RATIO} + 2.75 \times \text{RGI} - 1.86 \times \text{NIR}$	0.51	< 0.0001
Herschel	Site-specific	$\ln(\text{bm}) = 8.39 - 8.37 \times \text{RATIO} + 2.91 \times \text{RGI} - 2.01 \times \text{NIR}$	0.51	< 0.0001
	Cross-site	$\ln(\text{bm}) = 7.26 - 6.07 \times \text{RATIO} - 5.03 \times \text{RED} - \text{EDGE}$	0.75	< 0.0001
Tiksi	Site-specific	$\ln(\text{bm}) = 2.89 + 4.69 \times \text{NDVI} - 4.43 \times \text{RED} - \text{EDGE}$	0.68	< 0.0001
	Cross-site	$\ln(\text{bm}) = 9.50 - 17.0 \times \text{RATIO} + 35.8 \times \text{RED} - 8.71 \times \text{NIR}$	0.63	< 0.0001
	Site-specific	$\ln(\text{bm}) = 8.57 - 14.24 \times \text{RATIO} + 25.76 \times \text{RED} - 5.55 \times \text{NIR}$	0.66	< 0.0001

855

856

857 Table 6. Average satellite spectra based biomass estimate in the study plots (Plot), root
 858 mean square error of the biomass-satellite spectra model (RMSE), and average biomass
 859 estimate in the overall landscape for each study site. In the “Regression combination”
 860 column, ss refers to site-specific and cs to cross-site model, with first acronym pointing
 861 to biomass-cover/height regression and second acronym to biomass-satellite spectra
 862 regression. Combinations subplot-ss and subplot-cs refer to alternative biomass-satellite
 863 spectra regressions that use harvested biomass instead of cover/height modelled
 864 biomass as the response variable. In cs-cs and subplot-cs combinations, regressions
 865 were carried out with data from all study sites, but RMSE is calculated based on study
 866 site specific training and fitted data. Water bodies were masked out of the images before
 867 calculating the average landscape biomass.

Regression combination	Sodankylä			NW Russia			Herschel			Tiksi		
	Plot bioma ss (g m ⁻²)	RMSE (g m ⁻²)	Landsca pe biomass (g m ⁻²)	Plot bioma ss (g m ⁻²)	RMSE (g m ⁻²)	Landsca pe biomass (g m ⁻²)	Plot bioma ss (g m ⁻²)	RMSE (g m ⁻²)	Landsca pe biomass (g m ⁻²)	Plot bioma ss (g m ⁻²)	RMSE (g m ⁻²)	Landsca pe biomass (g m ⁻²)
ss-ss	291.9	150.0	315.2	392.7	485.9	477.5	185.1	71.9	222.8	154.6	48.5	151.4
cs-ss	317.9	171.8	341.4	388.3	480.8	469.3	156.2	43.9	191.4	158.8	54.3	154.1
cs-cs	384.2	234.1	290.5	342.9	509.8	367.5	359.8	222.6	428.9	128.2	75.1	132.1
subplot-ss	287.4	231.1	360.4	505.1	535.2	587.5	213.5	94.9	262.2	144.8	70.6	141.6
subplot-cs	335.9	237.5	342.6	617.8	584.4	442.5	230.6	258.9	718.1	158.9	87.1	183.0

868

869